Journal Name

Dynamic Article Links ►

Cite this: DOI: 10.1039/c0xx00000x

www.rsc.org/xxxxxx

ARTICLE TYPE

Electroless deposition and characterization of Fe/FeOx nanoparticles on porous carbon microspheres: structure and surface reactivity

Paul Duffy,[a] Ronan J. Cullen,[a] Dilushan Jayasundara,[a] Deirdre M. Murphy,[a] Emiliano Fonda,[b] Paula E. Colavita*[a, c]

Received (in XXX, XXX) Xth XXXXXXXXX 200X, Accepted Xth XXXXXXXXX 200X
DOI: 10.1039/b000000x

There has been great interest in synthetic methods that yield supported iron and iron oxide nanoparticles in order to prevent aggregation and improve their transport properties, handling and surface reactivity. In this work we report on the use of electroless deposition methods for the synthesis of carbon-supported iron/iron-oxide (Fe/FeOx) nanoparticles. We have used carbon porous microspheres synthesized via ultraspray pyrolysis as carbon scaffolds for the nucleation and growth of iron nanoparticles. The reported electroless deposition approach results in composite Fe/FeOx/carbon microspheres of narrowly dispersed size. A combination of X-ray powder diffraction (XRD) and X-ray absorption spectroscopies (EXAFS and XANES) was used in order to determine the structure and composition of the Fe/FeOx/Carbon microspheres. Microspheres were found to display (14 ± 1)% iron content (w/w), whereby (12 ± 3)% of iron atoms were present as metallic iron and the remaining as maghemite (Fe_2O_3). Finally, we show that the removal capacity of Fe/FeOx/Carbon microspheres for Cr(VI) is (20 ± 2) mg g^{-1} and that the maximum surface density for Cr adsorbates is (60 ± 6) μg m^{-2}, thus suggesting that these are promising materials for the removal of water pollutants from aqueous solution.

1. Introduction

Iron and iron/iron-oxide nanoparticles (Fe/FeOx) have been the subject of intense investigation due to their numerous potential applications. Their magnetic properties make them attractive candidates for medical applications in imaging, drug delivery and hyperthermia therapeutic strategies,[1,2] as well as for sensing/labelling and magnetic manipulation of catalysts or waste.[3] Nanosized iron particles, in comparison to micron-sized or bulk iron, possess higher surface to volume ratios that can lead to enhanced performance in heterogeneous catalysis. It has been argued that, beyond providing an increase in available reactive surface, nanosized iron particles can also display higher reactivity than macroscopic particles because of a combination of quantum effects and higher structural disorder.[4] Metallic iron nanoparticles also act as excellent electron donors in water and their use as agents for the reductive remediation of pollutants in the subsurface, ranging from metals to harmful anions and organic compounds, has been recently the subject of intense investigation in environmental chemistry.[5-7]

In order to take full advantage of the desirable properties of Fe and Fe/FeOx nanoparticles for any of the above applications, however, it is necessary to control their agglomeration. Magnetic particles tend to form large aggregates that render their magnetic manipulation and handling extremely challenging. Aggregation can also lead to a decrease of available surface area which has important implications for applications that rely on the surface reactivity of these iron materials. Furthermore, aggregation can severely decrease particle mobility and transport thus affecting the ability to deliver them through complex media; this problem is particularly important for environmental applications in subsurface remediation, where aggregation and filtering by porous soil matrices is a limiting factor for the effective implementation of nanosized iron technology.[6] In order to minimize aggregation problems and facilitate transport and delivery several research groups have adopted surface modification strategies to increase electrostatic or steric repulsions between particles. For instance, stabilization of Fe or Fe/FeOx nanoparticles has been achieved using surfactants,[8] polyelectrolytes,[9] synthetic polymers[10] and biopolymers.[11,12] However, an improvement in dispersion stability often occurs at the expense of reactivity, since surface modifiers also have the effect of blocking surface reactive sites. For this reason, it is often necessary or preferable to support unmodified nanoparticles on solid materials, such as clays,[13] carbon[14-17] or silica particles instead,[18] so that they can be readily handled/delivered while preserving their surface chemistry.

Supported Fe and Fe/FeOx nanoparticles are typically synthesized via solution methods in the presence of a large excess of solid support. Recently, electroless deposition has emerged as a strategy for the synthesis of nanostructured materials. Historically this technique was utilized for the growth of smooth and conformal metallic layers on conductive or insulating materials, whereby a surface catalysed reaction is leveraged in order to confine deposition to the surface.[19] However, it has

recently been shown that electroless deposition can also be optimized for the growth of anchored nanoparticles. Using electroless deposition, for instance, Metz et al. have synthesized nanostructured composite Au/C and Pt/C electrodes for energy storage and conversion applications.[20-22] Recently, we have shown that green electroless reduction agents can be used to deposit Ag and Pd nanoparticles.[23] In this work we report on the synthesis and characterization of composite Fe/C nanostructured materials obtained via an electroless deposition process. Electroless deposition of iron is challenging due to the low reduction potential of both Fe(II) and Fe(III). Nakanishi and co-workers have shown that dimethylamino borane (DMAB), a reductant complex used in industrial electroless plating processes, can be used for the electroless deposition of uniform iron films.[24] In this work we demonstrate that a modified DMAB-based process can be used to direct the synthesis of iron/iron-oxide nanoparticles at the surface of porous carbon microspheres with negligible formation of unsupported particles.

We have used ultrasonic spray pyrolysis (USP), to synthesize porous carbon microsphere (CMs) scaffolds with high specific surface area and narrow size distribution centered at ~700 nm as nanoparticle supports/carriers. The Tufenkji-Elimelech model predicts that filtration effects are minimized for particles between 0.1 μm and 1 μm in diameter;[25] therefore, CM size is in the optimal range for applications requiring delivery of nanoparticles through porous matrices. Using electroless deposition we controllably grew supported iron/iron-oxide nanoparticles in the range 10-20 nm on CMs and characterized them in terms of morphology and composition. Finally, we show that these Fe/CM composite particles display surface reactivity towards the remediation of Cr (VI), a toxic pollutant.

2. Experimental

Reagents

Reagent grade tin chloride dihydrate (96%; Fisher), palladium chloride (Fisher), sodium hydroxide (97%, Sigma), dichloroacetic acid (DCA, 99%, Sigma Aldrich), sulphuric acid (95%), hydrogen peroxide (30%, Sigma), dimethylamine borane complex (DMAB, 97%, Sigma), trifluoroacetic acid (TFA, 99%, Sigma), iron (III) sulfate hydrate (97%, Sigma), sodium dichromate dihydrate (99.5%, Sigma). Amorphous carbon samples used for XPS and X-ray diffraction studies were prepared via magnetron sputtering deposition techniques, as previously described by Cullen et al.[26] Amorphous carbon thin films were subsequently immersed in piranha solution (3:1, H_2SO_4 to H_2O_2) in order to increase the number of carboxylic acid moieties at their surface (*WARNING: Piranha solution should be handled with caution; it is a strong oxidant and reacts violently with organic materials. It also presents an explosion danger. All work should be performed under a fume hood*).

Carbon microsphere synthesis

Carbon microspheres (CMs) were synthesized using ultrasonic spray pyrolysis as previously reported. This method involves using a 1.67 MHz piezoelectric disk in order to nebulise a 1.5 M sodium dichloroacetate (NaDCA) precursor solution into a mist of droplets with narrow size distribution. Droplets were carried into a tube furnace by a flow of Ar, where the precursor undergoes pyrolysis at 700 °C. CMs thus generated (see Figure 1) were collected in a bubbler containing Millipore water; they were then filtered and washed with abundant water and ethanol and left to dry prior to further use.

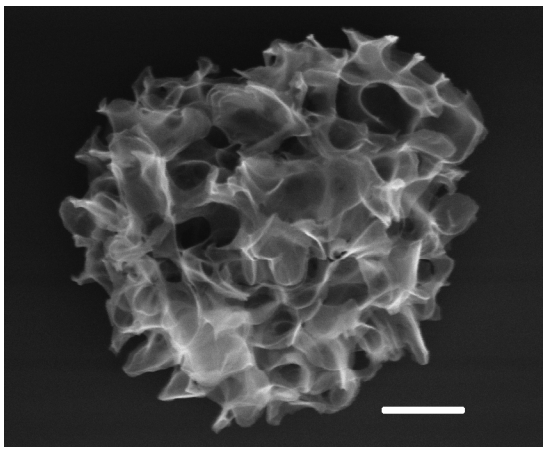

Figure 1. SEM image of a typical microsphere prepared via USP from 1.5 M NaDCA precursor solutions; scalebar = 600 nm.

Sensitisation and activation step

A solution 0.050 M in $SnCl_2$ and 0.070 M in trifluoroacetic acid was prepared and CMs were added to a final concentration of 0.2400 g/L and sonicated to obtain a uniform dispersion. CMs were left in the solution for approximately 30 min, subsequently filtered through 0.45 μM nylon membranes and washed with water and ethanol. CMs were then dispersed via sonication in a 5.6×10^{-3} M solution of $PdCl_2$ acidified to pH 1 via addition of HCl. After 30 min in this solution CMs were washed via multiple cycles of centrifugation and gentle stirring in Millipore water.

Iron nanoparticle growth

Water was heated up to 80 °C in a reflux apparatus prior to adding iron (III) sulfate to a concentration of 4.4×10^{-4} M; a typical batch size in our experiments was 50 mL. Freshly sensitized and activated CMs were then added to the hot solution to a concentration of approximately 0.1200 g/L, to which DMAB was added to a final concentration of 0.070 M. The CM dispersion was left at 80 °C for 1.5 h under reflux, constant stirring and under an Ar flow. The iron-modified CMs were filtered and washed with abundant degassed water and ethanol prior to drying and further characterization; samples were kept under an Ar flow at all times during filtering, washing and drying.

Characterization

Scanning Electron Microscopy (SEM) was carried out on a Zeiss Ultra microscope at an accelerating voltage of 10 keV. X-ray photoelectron spectroscopy (XPS) was performed under ultrahigh vacuum on an Omicron system with base pressure 1×10^{-10} bar, equipped with a monochromatized Al Kα source and a multichannel detector. X-ray diffraction (XRD) was carried out on a Siemes D500 diffractometer with monochromated Cu Kα radiation. Thermal Gravimetric Analysis (TGA) measurements were performed using a Perkin-Elmer Pyris 1 TGA, using air as a carrier gas and a heat ramp of 10 °C/min from 25°C to 900°C including two 5 min long isothermal steps at 100 °C and 200 °C. The specific surface area of carbon spheres was determined via Brunauer-Emmett-Teller (BET) analysis (Quantachrome Nova Station) using a multi-point BET plot.[27] The sample was pre-treated at 30 °C under vacuum for 24 h prior to analysis using N_2

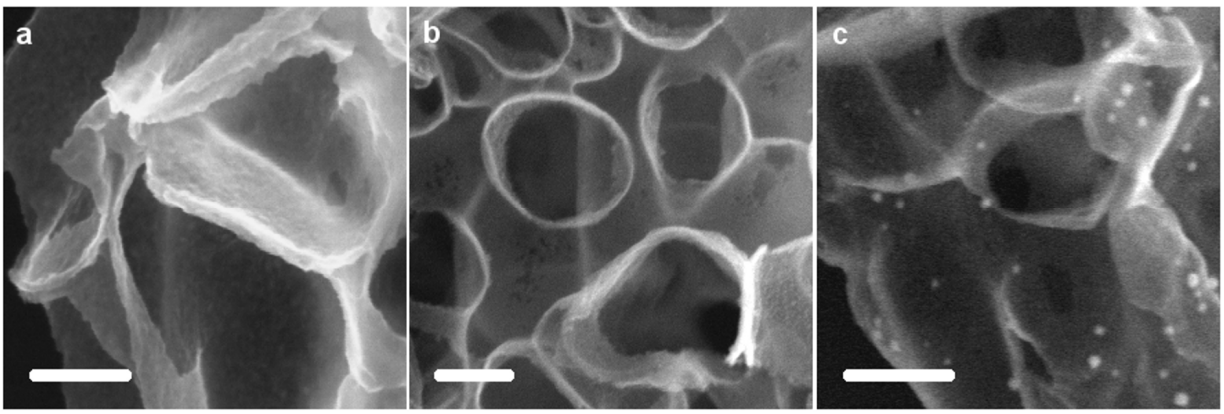

Figure 2. SEM images of the surface of carbon microspheres as prepared (a), after sensitization in a Sn^{2+} solution (b), and after activation in a Pd^{2+} solution (c); scalebar = 200 nm. After activation it is possible to observe the formation of small clusters decorating the surface of the carbon scaffold.

as the adsorbing gas. UV-Vis spectra of chromate anions were obtained on a Shimadzu UV- 2401PC.

Extended X-ray Absorption Fine Structure (EXAFS) spectra were collected at the SAMBA beamline at SOLEIL synchrotron.[28] The beamline was operated with a Si (220) double-crystal sagittal focusing monochromator. A pellet of pure Fe/CM powder was measured in transmission at the Fe K-edge; the pellet was checked for homogeneity with X-rays to estimate possible thickness errors. Data were analyzed using Horae[29] and FEFF8.4.[30] FEFF theoretical standards were tested versus experimental Fe_2O_3 and bcc-Fe standards. Maghemite, Hematite and Magnetite XANES standards were recorded on BM30 (ESRF) and calibrated on a Fe foil and a Hematite standard to match spectra recorded on SAMBA (SOLEIL).

Cr (VI) removal studies

A 12.9 mg/L Cr (VI) solution was degassed via ultrasonic treatment. Freshly prepared Fe/CM particles were added to 20mL of this Cr (VI) solution, in order to achieve a final composite concentration of 0.165 g/L. The suspension was then kept under an Argon atmosphere with constant stirring for the duration of our studies; the solution remained at neutral pH over the course of adsorption reactions. Aliquot samples were withdrawn at various time intervals. Subsequent quenching of the reaction was performed via filtration of the solution through 0.45 μM nylon membrane filters. The Cr (VI) concentration was measured via UV-ViS spectroscopy by monitoring the absorbance at 339 nm, according to a method developed by McCreery and co-workers.[31] Control adsorption experiments were carried out using 0.070 g/L suspensions of pristine carbon microspheres; this concentration was found to yield an equivalent particle number density to that used in Fe/CM adsorption experiments, as determined via TGA.

3. Results and Discussion

Carbon particles used in our experiments were synthesized via ultraspray pyrolysis using a protocol developed by Skrabalak et al.[32] and experimental conditions reported in our previous work.[33] Briefly, ultraspray pyrolysis synthesis from 1.5 M solutions of NaDCA precursors resulted in microspheres with diameter 1.8 ± 0.5 μm, as determined via SEM microscopy;[23] Figure 1 shows an SEM image of a microsphere. Particles thus prepared have high contents of graphitic carbon (>80% sp^2) and oxidized carbon groups (carboxylic and carboxylate groups),[33] and BET analysis shows that their specific surface area is 473 m^2/g.

In order to obtain iron nanoparticles supported on carbon microspheres, CMs underwent a two-step process of sensitization and activation prior to iron reduction at their surface via an electroless process. The proposed mechanism for the sensitization and activation steps consist of two steps.[34] First, an exchange of Sn^{2+} ions at the carbon surface, thanks to the presence of charged oxidized groups, such as carboxylates. Second, a reduction of Pd^{2+} to Pd^0 that takes place at the adsorbed Sn^{2+} sites, leading to the formation of small metallic Pd particles. These Pd^0 sites then serve as catalytic centers for the electroless deposition of metals. Figure 2a, b and c show the changes observed at the surface of CMs after each of these steps. After sensitization with Sn^{2+} we observe no morphological changes at the carbon surface, as shown by comparing the bare carbon surface in Figure 2a with the image after sensitization in Figure 2b. After the activation by immersion in the Pd^{2+} solution, formation of small clusters <5 nm in size is observed, as illustrated in Figure 2c.

Chemical changes taking place during the sensitization/activation steps at the surface, were investigated via XPS measurements. Figure 3 shows an XPS spectrum obtained on a graphitic amorphous carbon surface after the same sensitisation/activation steps described above. The spectrum shows the characteristic C 1s peak arising from the underlying carbon film at 284.5 eV.[26] The 3d doublet of Pd is visible at 340.5 and 335.5 eV, confirming the presence of metallic Pd at the carbon surface, probably with small amounts of adsorbed oxygen.[35,36] The Pd 3p doublet is also

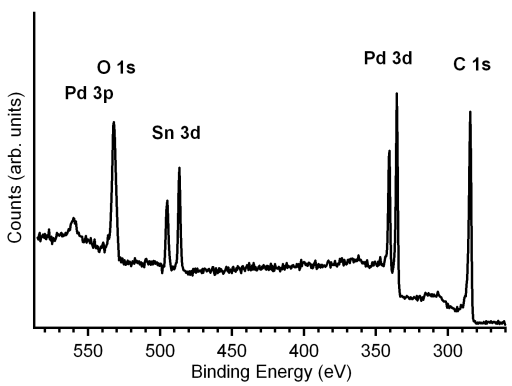

Figure 3. XP spectrum of carbon microspheres after undergoing the two step sensitization/activation process that nucleates Pd^0 nanoparticles at the carbon surface (a SEM image of these samples in shown in Figure 2c).

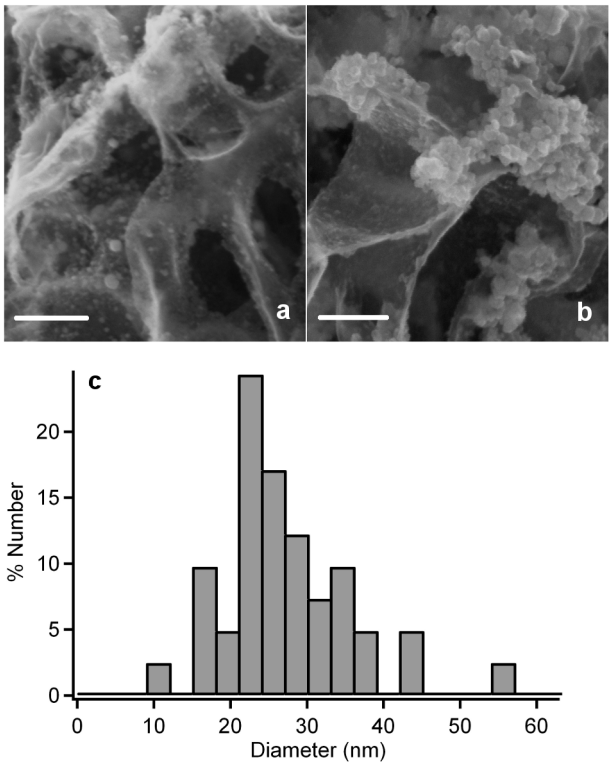

Figure 4. Typical SEM images of CMs obtained after deposition in DMAB/Fe^{2+} solution after 0.5 h (a) and after 1.5 h (b); scalebar = 200 nm. The size of primary particles increases with deposition time. (c) Size distribution of iron clusters obtained after 1.5 h of deposition.

visible at 532/560 eV, but it overlaps with the O 1s peak at approximately the same binding energy.[36] The spectrum also shows a doublet at 486.5/495.0 eV that we assign to Sn 3d arising from oxidized tin species.[37,38] Our results are consistent with previous XPS studies of the two-step sensitization/activation process on insulating materials, that show that oxidized tin species remain at the surface together with metallic Pd.[34] XPS data in figure 3 together with SEM characterization shown in Figure 2 therefore suggest that a two-step sensitization/activation process on CMs leads to the formation of Pd^0 catalytic seeds at nanostructured carbon surfaces.

After sensitization/activation, carbon microspheres were immersed in a solution containing Fe^{3+} at 80 °C, to which DMAB was added in order to lead to the reduction of Fe^{3+}. Figure 4a and 4b show the CM surface after 0.5 and 1.5 h, respectively, in the iron deposition solution. The images shows the presence of nanoparticles uniformly decorating the carbon scaffold. After 0.5 h in the deposition bath there is a large population of particles < 5 nm in diameter that accounts for the majority of particles that can be discerned in the images, as well as larger particles with a diameter of 13 ± 4 nm, as measured from SEM images. After 1.5 h nanoparticles increase in size to a diameter of 27 ± 8 nm; these primary particles often grow into aggregates that remain anchored at the carbon scaffold. Figure 4c shows the size distribution of particles obtained after 1.5 h in the DMAB/Fe^{3+} bath, determined from SEM images. The nanoparticles that decorate the porous carbon microspheres are not evident prior to the iron deposition step, thus suggesting that particle growth occurs due to electroless deposition of an iron-containing species.

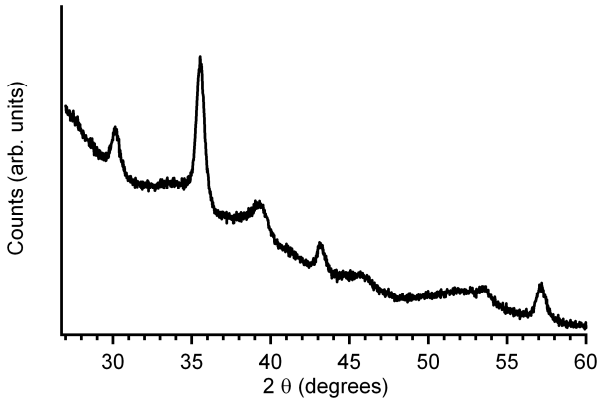

Figure 5. XRD pattern obtained after sensitization/activation and deposition in DMAB/Fe^{2+} solutions for 1.5 h on CM powders.

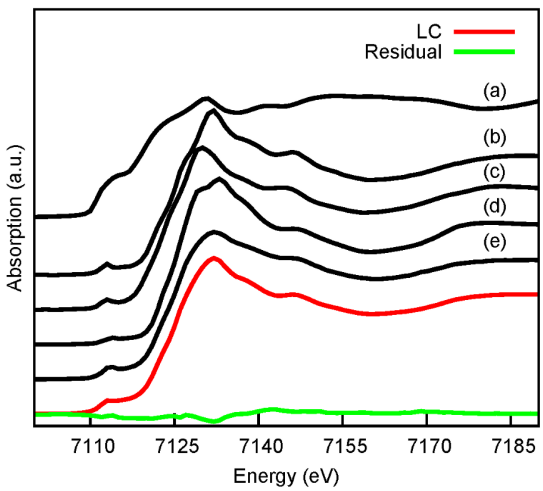

Figure 6. Fe K-edge absorption threshold obtained from (a) α-Fe, (b) hematite, (c) magnetite and (d) maghemite standards compared to that of (e) Fe/CM. The linear combination (LC) fit with the parameters reported in Table 1 and the residual are drawn in the bottom traces.

The composition of metal/carbon composite microspheres was investigated first via powder XRD measurements on Fe-decorated carbon samples. Figure 5 shows an XRD pattern of composite Fe/CM powders obtained after 1.5 h deposition. The pattern clearly shows the presence of iron oxides: the lines at 30.2°, 35.5°, 43.2°, 53.6° and 57.1° match the characteristic (220), (311), (400), (422) and (511) reflections of magnetite (Fe_3O_4; JCPDS file no.19-629) or maghemite (γ-Fe_2O_3; JCPDS file no. 25-1402) [39,40] and yielded a lattice constant of 8.37 Å, a value that falls between those of maghemite and magnetite.[41] Both of these oxides have spinel structure and yield similar XRD patterns which cannot be easily distinguished.[42] Additional broad lines suggest that other oxide phases with poor crystallinity contribute to the XRD pattern.[41,42] The presence of α-Fe (bcc) could not be detected in any of the powder samples, as indicated by the absence of a (110) line at 44°; this was somewhat surprising given that the same electroless deposition process, when used to deposit thick films at flat carbon substrates, yielded a (110) α-Fe reflection, in agreement with results by Nakanishi et al.[24] XRD results on microsphere samples therefore suggest that either metallic iron is not formed or it is present below the limit

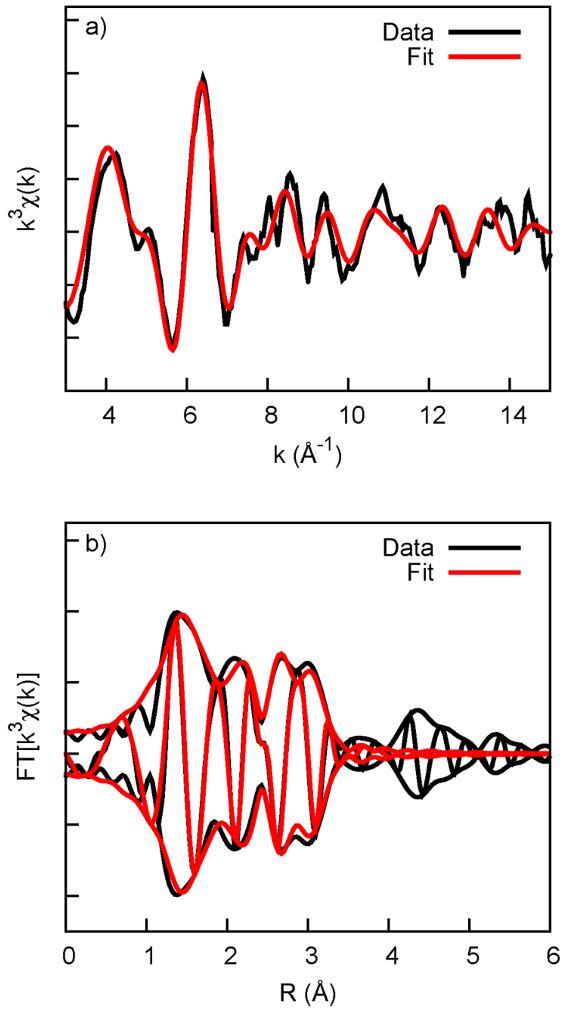

Figure 7. k^3-weighted EXAFS data of Fe/CM compared to the fitting curve in *k*-space (a) and *R*-space (b). The model did not include distances larger than 0.35 nm.

Components	**Fraction**
α -Fe	0.18(5)
Hematite (Fe_2O_3)	0.38(5)
Maghemite (γ-Fe_2O_3)	0.44(5)
Magnetite (Fe_3O_4)	0.00(5)

Table 1. Results of a linear combination fit on XANES data of Fe/CM sample (see Figure 6). Error bar is reported in brackets.

Path	**C.N.**	**R (nm)**	**σ^2 (10^{-5} nm^2)**
O1 (oxide)	4.6(9)	0.195(2)	13(3)
Fe1 (α-Fe)	0.7(2)	0.251(2)	7(1)
Fe2 (α-Fe)	C.N.(Fe1)/8*6	0.290(3)	
Fe3 (oxide)	2.6(5)	0.299(2)	
Fe4 (oxide)	C.N.(Fe3)	0.343(2)	

Table 2. Summary of scattering paths obtained from a best fit of the EXAFS spectrum of Fe/CM powders.

of detection when carbon microspheres are used as scaffolds for electroless deposition. Also, XRD results indicate that iron oxide/s (either Fe_2O_3 or Fe_3O_4) are present at the carbon surface; oxides could originate from air exposure after deposition and isolation of Fe/CM microspheres[43] or even result from metal hydroxide formation during DMAB electroless deposition.[24,44,45]

In order to better understand composition and structure of Fe/CM particles, we carried out X-ray absorption spectroscopy (XAS) measurements. In contrast with XRD, XAS can provide structural and composition information independently from the presence of long range order and is therefore better suited for characterizing disordered iron and iron oxide phases. Furthermore, XAS is sensitive to metal oxidation state and can be used to distinguish oxide phases with similar lattice structures as is the case with maghemite and magnetite.[46] We measured the XAS spectrum of Fe/CM and of iron oxide standards; Fe/CM samples were prepared under the same conditions, dried and kept in air for several weeks prior to XAS measurements. The absorption edge jump was used to estimate an iron content of 14 ± 1 % by weight, the pellet was checked for homogeneity with x-rays to estimate possible thickness errors. Figure 6 shows the Fe K-edge absorption threshold obtained from our sample compared to standards; a linear combination fit of the normalized XANES spectrum including all combinations of metallic iron, hematite, maghemite and magnetite was performed and the results are shown in Table 1: under all models, the magnetite is excluded, while hematite and maghemite have similar weights with a non negligible fraction of α-Fe. These results indicate that Fe is present mainly in two forms Fe^{3+} and Fe^0.

EXAFS data analysis was performed in R-space including single scattering contributions of Fe_2O_3 and α-Fe up to 0.35 nm. Again, it is possible to distinguish the presence of α-Fe mixed with one or more Fe^{3+} oxides. Several parameters where constrained as far as physically meaningful. The α-Fe fraction was left free as well as the lattice parameter, this means that coordination numbers and distances for Fe1 and Fe2 in Table 2 are linked by a factor. A similar approach has been used for the oxide phase, but since its signal is stronger, distances of separate shells are let independent in the refinement. It is unlikely to defintely distinguish between maghemite[47] and hematite[48] on the basis of this fit, but it is tempting to compare distances reported in Table 2 with those reported for micro or nano maghemite particles by Corrias et al.:[49] Fe-O1 at 0.192 nm, Fe-Fe1 at 0.299 nm, Fe-Fe2 0.344 nm, while the same authors found for hematite: Fe-O1 at 0.194 nm, Fe-O2 at 0.210 nm, Fe-Fe1 at 0.289 nm, Fe-Fe2 at 0.297 nm, Fe-Fe3 at 0.336 nm, Fe-Fe4 at 0.370 nm and Fe-Fe5 at 0.398 nm. The correspondence of the EXAFS data of the oxide fraction with micro or nano maghemite is striking. Assignment of the oxide phase to maghemite is also in agreement with XRD patterns which did not show the presence of hematite in electrolessly deposited Fe/CM samples. Finally, results confirm the presence of at least 12 ± 3 % of Fe^0 which is in good agreement with the fraction reported in Table 1 obtained from XANES data. Taking into account a 14% (w/w) iron content, this result suggests that the Fe^0 content is approximately 1.7% by weight; this value is below typical limits of detection for XRD of crystalline phases in amorphous matrices (>2%)[50] and it explains our inability to resolve Fe^0 lines in XRD patterns of Fe/CM particles.

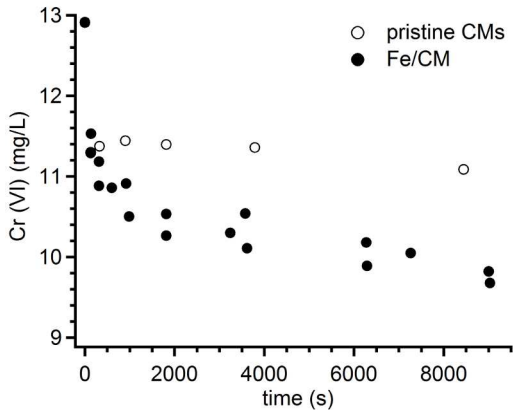

Figure 8. Cr (VI) removal from solution as a function of time for pristine CM (○) and Fe/CM particles (●).

Following the structural characterisation of Fe/CM microspheres we investigated their properties for the removal of pollutants. The removal of Cr (VI) species, in particular, is of utmost importance in water treatment processes due to the toxic properties of this high-valent metal species; carbon particles, iron and iron oxides have all been used in order to remediate Cr (VI) contaminated waters. Therefore, we decided to investigate whether our composite particles, which contain these three types of materials, could remove Cr (VI) from aqueous solutions.

The removal curves shown in Figure 8 (trace ●) indicate that when Fe/CM composite microspheres are added to an aqueous solution of Cr (VI), the concentration of this pollutant decreases as a function of time in the aqueous phase. In order to compare the removal capacity of Fe/CM particles to that of bare carbon microspheres, we carried out control adsorption experiments using pristine CMs. The concentration of carbon particles used in the controls was chosen in order to match the number density of Fe/CM used in Cr (VI) adsorption experiments. Figure 8 shows the result of a control experiment using pristine carbon microsphere suspensions (trace ○): the adsorption curve indicates that the maximum removal capacity of an equivalent quantity of carbon microspheres is lower than that of Fe/CM particles. An interpolation of adsorption curves using exponentials yielded maximum adsorption capacities for carbon microspheres and Fe/CM particles under our experimental conditions of (22 ± 1) mg g^{-1} and (20 ± 2) mg g^{-1}, respectively.

The adsorption capacity of pristine carbon microspheres is within the range of carbon adsorbents[51] and comparable to that of activated carbon particles.[52,53] This result suggests that carbon particles prepared via USP from NaDCA precursors are promising reactive/adsorbing scaffold materials for Cr (VI) removal. Normalization by the specific surface area of NaDCA particles yielded a maximum surface density value for adsorbed Cr at the pristine carbon surface of (46 ± 2) μg m^{-2}. The BET area of Fe/CM particles was found to be 335 m^2 g^{-1}, thus yielding a maximum surface density of adsorbed Cr of (60 ± 6) μg m^{-2}. This result indicates that the surface of Fe/CM composite particles is ~30% more effective on average than that of carbon alone at capturing Cr (VI) from solution under the same conditions.

Both metallic Fe^0 and iron oxides can contribute to the removal of Cr (VI) from solution albeit via different mechanisms. Metallic iron can reduce Cr (VI) to less mobile Cr (III) species, as shown by the work of numerous groups on the use of iron nanoparticles in water remediation.[5,12,54,55] The reductive properties of iron nanoparticles can also be enhanced via Pd-doping of iron nanoparticles,[5] however, it is not possible to establish whether Pd present in our electrolessly deposited particles enhances the removal capacity of Fe/CM composites, based on the present results alone. Iron oxides can remove metal contaminants via a process of surface complexation and ion exchange;[42,56-58] hydrated iron oxide surfaces are, in fact, excellent at complexing and sequestering both Cr (VI) and Cr (III) species from solution and have been extensively used in the treatment of waste waters contaminated with chromate.[42] Assuming that the enhanced adsorption observed in Figure 8 arises entirely from the presence of Fe_2O_3, and using %weight contents determined via XANES, we can estimate that the removal capacity of Fe_2O_3 oxides in Fe/CM particles is approximately 46 mg g^{-1}. This value is extremely high compared to typical Cr (VI) removal capacities: Zhong et al.,[58] for instance, reported values of 3.86 mg g^{-1} and 4.75 mg g^{-1} for pure maghemite and hematite nanostructures, whereas Hu et al.[59] achieved maximum removals of 20 mg g^{-1} for synthesized maghemite nanoparticles. This suggests that high surface availability due to anchoring at the carbon scaffold and/or a simultaneous reductive removal mechanism might also contribute to the high adsorption capacities observed for our supported Fe/FeOx particles.

Conclusions

We have shown that electroless deposition methods can be used to deposit iron nanoparticles at the surface of porous carbon microspheres. We have used a combination of electron microscopy, X-ray photoelectron spectroscopy, X-ray diffraction and X-ray absorption techniques in order to determine morphology and composition of the resulting inorganic nanoparticles. We show that the nanostructured deposits obtained via electroless deposition consist of mixed metallic and oxide phases. Analysis of X-ray absorption edge and fine structrure (XANES and EXAFS) were essential in order to both detect the presence of metallic iron and to determine that the majority of the oxide phase consisted of maghemite.

Adsorption experiments indicate that Fe/CM particles prepared via electroless deposition are highly effective at removing chromate from aqueous solutions. Fe/CM particles were shown to perform better than the carbon scaffold alone. The Cr (VI) removal mechanism is expected to result from the combination of reductive and adsorptive processes, given that Fe^0, maghemite and carbon are all three present and potentially active towards chromate capture from solution. These mixed material microspheres appear to be promising for the design of new adsorptive/reactive agents in environmental remediation. Furthermore, we envision that the ability to anchor Fe/FeOx nanoparticles at carbon microparticle surfaces could be advantageous in order to improve handling, aggregation and transport properties of nanosized iron-based materials.

Acknowledgements

This publication has emanated from research conducted with the

financial support of the Environmental Protection Agency (EPA) Ireland, under grant No.2008-PhD-WRM-2 and of Science Foundation Ireland under grant No. 09/RFP/CAP2174. We thank Dr. S. Reguerr of Synchrotron SOLEIL for recording XANES standards on BM30 (ESRF) and for helpful discussions. The authors are also grateful to Profs. C. McGuinness and I. Shvets for granting access to XPS instrumentation.

Notes and references

[a] *School of Chemistry, University of Dublin Trinity College, College Green, Dublin 2, Ireland. Email: colavitp@tcd.ie*
[b] *Synchrotron SOLEIL, L'Orme des Merisiers, Saint-Aubin, F-91192 Gif-sur-Yvette Cedex, France.*
[c] *Centre for Research on Adaptive Nanostructures and Nanodevices (CRANN), University of Dublin Trinity College, College Green, Dublin 2, Ireland.*

1. D. L. Huber, *Small*, 2005, **1**, 482.
2. S. C. McBain, H. H. P. Yiu and J. Dobson, *Int. J. Nanomed.*, 2008, **3**, 169.
3. A. H. Lu, E. L. Salabas and F. Schuth, *Angew. Chem.*, 2007, **46**, 1222.
4. J. T. Nurmi, P. G. Tratnyek, V. Sarathy, D. R. Baer, J. E. Amonette, K. Pecher, C. Wang, J. C. Linehan, D. W. Matson, R. L. Penn and M. D. Driessen, *Environ. Sci. Technol.*, 2005, **39**, 1221.
5. X. Q. Li, D. W. Elliott and W. X. Zhang, *Crit. Rev. Solid State Mater. Sci.*, 2006, **31**, 111.
6. G. V. Lowry, in *Environmental Nanotechnology. Applications and impacts of nanomaterials*, eds. M. R. Wiesner and J.-Y. Bottero, McGraw-Hill, New York, 2007, pp. 297.
7. W. X. Zhang, *J. Nanopart. Res.*, 2003, **5**, 323.
8. S. R. Kanel, J. M. Greneche and H. Choi, *Environ. Sci. Technol.*, 2006, **40**, 2045.
9. B. W. Hydutsky, E. J. Mack, B. B. Beckerman, J. M. Skluzacek and T. E. Mallouk, *Environ. Sci. Technol.*, 2007, **41**, 6418.
10. N. Saleh, T. Phenrat, K. Sirk, B. Dufour, J. Ok, T. Sarbu, K. Matyiaszewski, R. D. Tilton and G. V. Lowry, *Nano Lett.*, 2005, **5**, 2489.
11. T. Liu, L. Zhao, D. Sun and X. Tan, *J. Hazard. Mater.*, 2010, **184**, 724.
12. Y. H. Xu and D. Y. Zhao, *Water Res.*, 2007, **41**, 2101.
13. Y.-H. Son, J.-K. Lee, Y. Soong, D. Martello and M. Chyu, *Chem. Mater.*, 2010, **22**, 2226.
14. J. Lee, D. Lee, E. Oh, J. Kim, Y. P. Kim, S. Jin, H. S. Kim, Y. Hwang, J. H. Kwak, J. G. Park, C. H. Shin and T. Hyeon, *Angew. Chem.*, 2005, **44**, 7427.
15. B. Schrick, B. W. Hydutsky, J. L. Blough and T. E. Mallouk, *Chem. Mater.*, 2004, **16**, 2187.
16. J. D. Atkinson, M. E. Fortunato, S. A. Dastgheib, M. Rostam-Abadi, M. J. Rood and K. S. Suslick, *Carbon*, 2011, **49**, 587.
17. B. Sunkara, J. Zhan, J. He, G. L. McPherson, G. Piringer and V. T. John, *ACS Appl. Mater. Interfaces*, 2010, **2**, 2854.
18. T. Zheng, J. Zhan, J. He, C. Day, Y. Lu, G. L. McPherson, G. Piringer and V. T. John, *Environ. Sci. Technol.*, 2008, **42**, 4494.
19. G. O. Mallory and J. B. Haydu, eds., *Electroless Plating: Fundamentals and applications*, American Electroplaters and Surface Finishers Society, Orlando, FL, 1990.
20. K. M. Metz, D. Goel and R. J. Hamers, *J. Phys. Chem. C*, 2007, **111**, 7260.
21. K. M. Metz, K. Y. Tse, S. E. Baker, E. C. Landis and R. J. Hamers, *Chem. Mater.*, 2006, **18**, 5398.
22. K. M. Metz, P. E. Colavita, K. Y. Tse and R. J. Hamers, *J. Power Sources*, 2012, **198**, 393.
23. P. Duffy, L. A. Reynolds, S. E. Sanders, K. M. Metz and P. E. Colavita, *Mater. Chem. Phys.*, 2013, in press.
24. T. Nakanishi, Y. Masuda and K. Koumoto, *J. Cryst. Growth*, 2005, **284**, 176.
25. N. Tufenkji and M. Elimelech, *Environ. Sci. Technol.*, 2004, **38**, 529.
26. R. J. Cullen, J. Cheng, G. DuFaure, D. Jayasundara, L. Soldi and P. E. Colavita, *Chem. Mater.*, 2012, **24**, 1031.
27. S. Brunauer, P. H. Emmett and E. Teller, *J. Am. Chem. Soc.*, 1938, **60**, 309.
28. V. Briois, E. Fonda, S. Belin, L. Barthe, C. La Fontaine, F. Langlois, M. Ribbens and F. Villain, "SAMBA: The 4–40 keV X-ray absorption spectroscopy beamline at SOLEIL", *UVX 2010 - 10e Colloque sur les Sources Cohérentes et Incohérentes UV, VUV et X ; Applications et Développements Récents*, 2011.
29. B. Ravel and M. Newville, *J. Synchrot. Radiat.*, 2005, **12**, 537.
30. A. L. Ankudinov, A. I. Nesvizhskii and J. J. Rehr, *Phys. Rev. B*, 2003, **67**, 115120.
31. L. Xia, E. Akiyama, G. Frankel and R. McCreery, *J. Electrochem. Soc.*, 2000, **147**, 2556.
32. S. E. Skrabalak and K. S. Suslick, *J. Am. Chem. Soc.*, 2006, **128**, 12642.
33. P. Duffy, L. M. Magno, R. Yadav, S. Roberts, A. D. Ward, S. W. Botchway, P. E. Colavita and S. J. Quinn, *J. Mater. Chem.*, 2012, **22**, 432.
34. M. Charbonnier, M. Alami and M. Romand, *J. Appl. Electrochem.*, 1998, **28**, 449.
35. G. K. Wertheim, S. B. Dicenzo and D. N. E. Buchanan, *Phys. Rev. B*, 1986, **33**, 5384.
36. K. S. Kim, A. F. Gossmann and N. Winograd, *Anal. Chem.*, 1974, **46**, 197.
37. R. O. Ansell, T. Dickinson, A. F. Povey and P. M. A. Sherwood, *J. Electrochem. Soc.*, 1977, **124**, 1360.
38. E. Paparazzo, G. Fierro, G. M. Ingo and N. Zacchetti, *Surf. Interface Anal.*, 1988, **12**, 438.
39. Y.-k. Sun, M. Ma, Y. Zhang and N. Gu, *Colloids Surf., A*, 2004, **245**, 15.
40. I.-M. Grabs, C. Bradtmöller, D. Menzel and G. Garnweitner, *Cryst. Growth Des.*, 2012, **12**, 1469.
41. U. Schwertmann and R. M. Cornell, *Iron Oxides in the Laboratory - Preparation and Characterization*, 2nd edn., Wiley-VCH, Weinheim, 2000.
42. R. M. Cornell and U. Schwertmann, *The iron oxides - Structure, properties, reactions, occurrence and uses*, 1st edn., VCH Publishers, Weinheim and New York, 1996.
43. S. Li, W. Yan and W.-x. Zhang, *Green Chem.*, 2009, **11**, 1618-1626.
44. S. Balci, A. M. Bittner, M. Schirra, K. Thonke, R. Sauer, K. Hahn, A. Kadri, C. Wege, H. Jeske and K. Kern, *Electrochim. Acta*, 2009, **54**, 5149.
45. V. M. Krutskikh, M. V. Ivanov, A. B. Drovosekov, E. N. Lubnin, B. F. Lyakhov and Y. M. Polukarov, *Prot. Met.*, 2007, **43**, 560.

46. A. Espinosa, A. Serrano, A. Llavona, J. J. d. l. Morena, M. Abuin, A. Figuerola, T. Pellegrino, J. F. Fernández, M. Garcia-Hernández, G. R. Castro and M. A. García, *Meas. Sci. Technol.*, 2012, **23**, 015602.
47. C. Pecharroman, T. Gonzalez-Carreno and J. E. Iglesias, *Phys. Chem. Miner.*, 1995, **22**, 21.
48. R. L. Blake, Hessevic.Re, T. Zoltai and L. W. Finger, *Am. Mineral.*, 1966, **51**, 123.
49. A. Corrias, G. Ennas, G. Mountjoy and G. Paschina, *Phys. Chem. Chem. Phys.*, 2000, **2**, 1045.
50. B. A. Sarsfield, M. Davidovich, S. Desikan, M. Fakes, S. Futernik, J. L. Hilden, J. S. Tan, S. Yin, G. Young, B. Vakkalagadda and K. Volk, *Adv. X-Ray Anal.*, 2005, **49**, 322.
51. M. Owlad, M. Aroua, W. Daud and S. Baroutian, *Water, Air, Soil Pollut.*, 2009, **200**, 59.
52. S. Babel and T. A. Kurniawan, *Chemosphere*, 2004, **54**, 951.
53. I. Han, M. A. Schlautman and B. Batchelor, *Water Environ. Res.*, 2000, **72**, 29.
54. S. M. Ponder, J. G. Darab and T. E. Mallouk, *Environ. Sci. Technol.*, 2000, **34**, 2564.
55. N. Melitas, O. Chuffe-Moscoso and J. Farrell, *Environ. Sci. Technol.*, 2001, **35**, 3948.
56. D. A. Dzombak and F. M. M. Morel, *Surface Complexation Modeling: Hydrous ferric oxide*, John Wiley & Sons, New York, 1990.
57. G. A. Waychunas, C. S. Kim and J. F. Banfield, *J. Nanopart. Res.*, 2005, **7**, 409.
58. L. S. Zhong, J. S. Hu, H. P. Liang, A. M. Cao, W. G. Song and L. J. Wan, *Adv. Mater.*, 2006, **18**, 2426.
59. J. Hu, G. Chen and I. M. C. Lo, *Water Res.*, 2005, **39**, 4528.

